Retromer-driven membrane tubulation separates endosomal recycling from Rab7/Ypt7-dependent fusion

Latha Kallur Purushothaman[a,†], Henning Arlt[a,†,‡,*], Anne Kuhlee[b], Stefan Raunser[b], and Christian Ungermann[a,*]

[a]Department of Biology/Chemistry, Biochemistry Section, University of Osnabrück, 49076 Osnabrück, Germany; [b]Department of Structural Biochemistry, Max-Planck Institute of Molecular Physiology, 44227 Dortmund, Germany

ABSTRACT Endosomes are the major protein-sorting hubs of the endocytic pathway. They sort proteins destined for degradation into internal vesicles while in parallel recycling receptors via tubular carriers back to the Golgi. Tubule formation depends on the Rab7/Ypt7-interacting retromer complex, consisting of the sorting nexin dimer (SNX-BAR) and the trimeric cargo selection complex (CSC). Fusion of mature endosomes with the lysosome-like vacuole also requires Rab7/Ypt7. Here we solve a major problem in understanding this dual function of endosomal Rab7/Ypt7, using a fully reconstituted system, including purified, full-length yeast SNX-BAR and CSC, whose overall structure we present. We reveal that the membrane-active SNX-BAR complex displaces Ypt7 from cargo-bound CSC during formation of recycling tubules. This explains how a single Rab can coordinate recycling and fusion on endosomes.

INTRODUCTION

Endosomes function as a general sorting station in the endocytic pathway of eukaryotic cells. They fuse with plasma membrane–derived endocytic vesicles carrying cell surface receptors and transporters, as well as with vesicles coming from the *trans*-Golgi network, which contain, for instance, immature lysosomal hydrolases in complex with their respective transport receptor (Huotari and Helenius, 2011). On the endosomal surface, each of the membrane cargoes is subsequently sorted according to their respective sorting mark. Ubiquitinated receptors are corralled by the endosomal sort-

ing complexes required for transport (ESCRT) machinery and incorporated into intraluminal vesicles (ILVs; Henne *et al.*, 2011), whereas transport receptors that dissociate from their bound hydrolase are found in tubular structures formed by the retromer complexes (Cullen and Korswagen, 2012; Seaman *et al.*, 2013). These unique membrane-sorting processes convert the endosome from an organelle with multiple tubules into a round multivesicular body that eventually fuses with the lysosome.

Endosomal biogenesis depends on controlled fusion events, which are mediated by a general machinery of Rab GTPases, tethering factors, and membrane-bound SNAREs (Kümmel and Ungermann, 2014). Rabs are prenylated switch-like proteins that exist in an inactive, GDP, and active, GTP, form. Upon GTP loading via a membrane-localized guanine nucleotide exchange factor (GEF), Rabs interact with effectors such as tethering factors (Barr, 2013). Tethers then seem to function as general bridges between vesicle and organelle membrane and assist the assembly of membrane-bound soluble *N*-ethylmaleimide–sensitive factor attachment protein receptors (SNAREs) into a stable four-helix bundle that drives fusion of the two lipid bilayers (Jahn and Scheller, 2006; Kümmel and Ungermann, 2014).

Endosomal maturation is accompanied by a change in the fusion machinery. Early endosomes initially carry Rab5 (or in yeast, Vps21) and the tethering complex CORVET. Due to the recruitment of the Mon1-Ccz1 GEF, Rab7 (or Ypt7 in yeast) is recruited to endosomes (Kinchen and Ravichandran, 2010; Nordmann *et al.*, 2010; Poteryaev *et al.*, 2010; Yousefian *et al.*, 2013; Singh *et al.*, 2014; Li *et al.*, 2015).
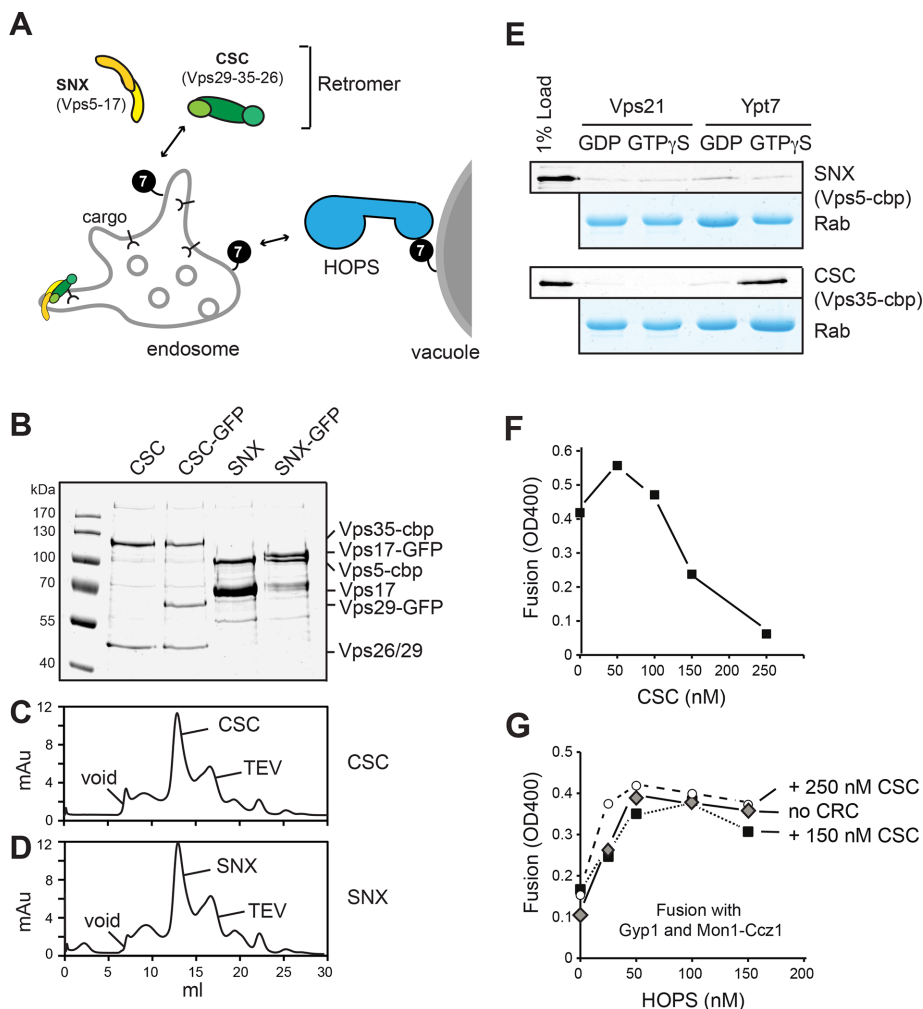
FIGURE 1: Purification of retromer subcomplexes. (A) Model of Ypt7 interaction with retromer subcomplexes and HOPS on endosomes and vacuoles. 7, Ypt7; CSC, cargo selection complex; SNX, sorting nexin BAR complex. (B–D) Analysis of purified retromer subcomplex. (B) Overproduced CSC and SNX-BAR complexes were purified via the C-terminal TAP tag on Vps35 (CSC) or the SNX subunit Vps5. SNX-GFP had in addition a C-terminal GFP on Vps17; a CSC-GFP Vps29 was tagged similarly. Complexes were analyzed via SDS–PAGE, and gels were stained with Coomassie. (C, D) Gel filtration of SNX-BAR and CSC. TEV eluates from IgG columns were applied to gel filtration as described in *Materials and Methods*. TEV indicates the migration of the tobacco etch virus protease used to elute the protein from IgG beads. (E) Interaction of purified CSC and SNX-BAR with Rabs. C-terminal GST-tagged Vps21 and Ypt7 Rabs charged with either GDP or GTPγS were immobilized on GSH beads and incubated with purified SNX-BAR and CSC complexes. Eluted proteins were analyzed by SDS–PAGE and Western blotting with antibodies against the calmodulin-binding peptide (cbp; top of displayed gel) or directly analyzed by Coomassie staining (bottom). (F, G) Effect of purified CSC complex on vacuole fusion. Purified vacuoles from the two tester strains were incubated in the presence of ATP for 90 min at 26°C in the presence of the indicated amount of purified CSC (F). In G, the nonspecific GAP Gyp1-46 and the Ypt7 GEF Mon1-Ccz were included in the vacuole fusion reaction. Fusion reactions contained either no CSC or two different amounts of inhibitory CSC concentrations based on the titration in F. HOPS was titrated into each assay as indicated, and fusion was assayed after 90 min at 26°C (see *Materials and Methods*).

In agreement, Mon1-Ccz1 colocalizes with Vps21 to endosomes (Rana *et al.*, 2015). In yeast, Rab5 inactivation requires the BLOC-1 complex and its interacting GTPase-inactivating protein Msb3 (Lachmann *et al.*, 2012; John Peter *et al.*, 2013; Rana *et al.*, 2015). This change in Rab seems to determine both fusion specificity and recruitment of sorting machineries. One such sorting machinery is the retromer complex, which, together with either SNX or SNX-BAR proteins, mediates recycling of transmembrane cargo receptors

back to the Golgi by formation of membrane tubules (Seaman, 2012; Burd and Cullen, 2014). Rab7 and Ypt7 are required for endosomal recycling and directly bind to retromer (Rojas *et al.*, 2008; Seaman *et al.*, 2009; Balderhaar *et al.*, 2010; Liu *et al.*, 2012; Priya *et al.*, 2015). However, the Rab itself was not present on the tubules (Arlt *et al.*, 2015b). Ypt7-GTP also interacts with the vacuolar homotypic fusion and vacuole protein sorting (HOPS) tethering complex, which is required for fusion of late endosomes with lysosomes in both yeast and metazoan cells (Balderhaar and Ungermann, 2013).

Early and late endosomes can be distinguished morphologically by electron microscopy (Prescianotto-Baschong and Riezman, 2002; Griffith and Reggiori, 2009), and the transition through these compartments can be traced by endocytosed cargo (Toshima *et al.*, 2006; Arlt *et al.*, 2015a). This analysis revealed that this cargo colocalized simultaneously with ESCRTs, retromer, the endosomal fusion machinery, and trace amounts of Ypt7, suggesting that the endosomal cargo-sorting machinery operates in parallel on maturing endosomes (Arlt *et al.*, 2015a). Considering that Ypt7 binds both retromer and the HOPS tethering complex, which mediates fusion (Wickner, 2010), Ypt7 availability could be a possible explanation of how maturation is sensed.

Here we address the key question of how a dually used Rab like Rab7/Ypt7 can support two distinct events on endosomes. Using purified, full-length retromer subcomplexes, CSC and SNX-BAR, we dissect the consecutive assembly of retromer complexes on membranes. We demonstrate that retromer complex formation on membranes releases Ypt7, which then becomes available for fusion. Our data can explain how a single endosomal Rab coordinates fission and fusion events during maturation.

RESULTS

Characterization of purified retromer subcomplexes

Yeast retromer has been purified as a heteropentamer (Seaman *et al.*, 1998), which is subdivided into two subcomplexes: the retromer, with its subunits Vps35, Vps26, and Vps29, here referred to as CSC; and the dimeric sorting nexin complex, with a curvature-inducing BAR domain (SNX-BAR) consisting of Vps5 and Vps17 (Seaman and Williams, 2002; Seaman, 2004; Figure 1A). The Vps5 and Vps17 proteins both have a putative unstructured N-terminal part followed by a phosphatidylinositol-3-phosphate (PI-3-P)–binding Phox-homology (PX) domain and a C-terminal BAR domain (Burda *et al.*, 2002; Seaman and Williams, 2002). Vps5, as well as the equivalent human SNX1 and SNX5, can tubulate membranes in vitro (van Weering *et al.*, 2012).
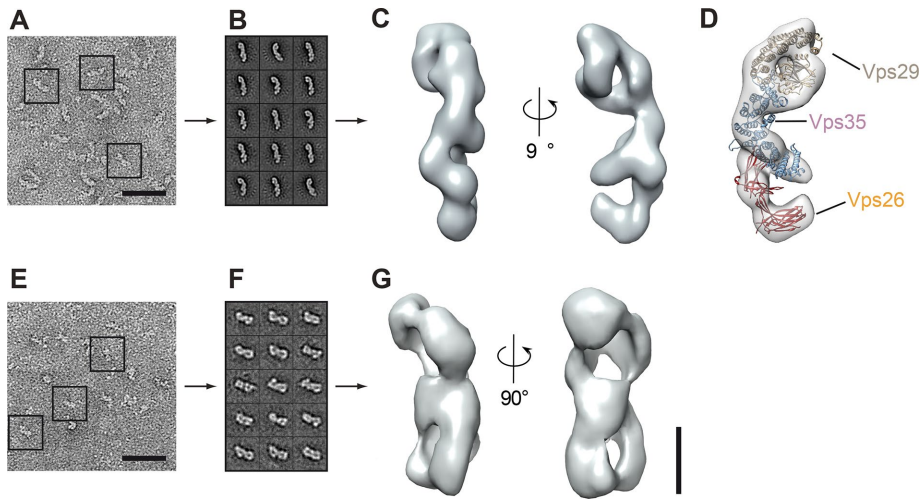
FIGURE 2: Molecular architecture of yeast CSC and SNX-BAR complexes. CSC and SNX-BAR complexes were purified via one-step purification from yeast (see *Materials and Methods*). Typical electron micrographs of (A) CSC and (E) SNX-BAR negatively stained particles corresponding to (B, F) 15 representative class averages (110–340 for CSC; 30–60 particles for SNX-BAR). Scale bars, 50 nm. (C, G) Two different views of CSC (C) and SNX-BAR (G). Three-dimensional reconstruction based on random conical tilt data. (D) Structures of Vps29, Vps35, and Vps26 (Collins *et al.*, 2005, 2008; Shi *et al.*, 2006; Hierro *et al.*, 2007) fitted into the density of yeast retromer. Scale bars, 50 Å.

We cooverexpressed all retromer subunits in a single yeast strain. Overproduced yeast SNX-BAR retromer could be purified as a heteropentamer but had the tendency to aggregate or disassemble during subsequent assays (Supplemental Figure S1). In contrast, both full-length SNX-BAR and CSC complexes were stable on gel filtration and reasonably clean enough to be used in subsequent assays (Figure 1, B and D).

As a first assay for functionality, we tested their interaction with endosomal Rabs, which were immobilized as glutathione S-transferase (GST) fusion proteins on glutathione beads. In agreement with previous findings (Rojas *et al.*, 2008; Seaman *et al.*, 2009; Balderhaar *et al.*, 2010; Liu *et al.*, 2012; Harrison *et al.*, 2014; Priya *et al.*, 2015), only CSC interacted with Ypt7-GTP (Figure 1E) and could inhibit the Ypt7-dependent vacuole fusion assay in a dose-dependent manner (Figure 1F). For the latter assay, vacuoles were purified from two tester strains that upon ATP-dependent in vitro fusion restored maturation of the immature alkaline phosphatase (Pho8) present in one vacuole population by supplying the protease present in second vacuole population (Haas *et al.*, 1994). The inhibition by CSC was efficiently quenched by purified HOPS complex (Figure 1G), suggesting that both compete for Ypt7 on vacuoles. Note that we included in this competition assay an unspecific GAP, Gyp1-46, and excess of the Ypt7-GEF Mon1-Ccz1 to make possibly inaccessible Ypt7 available for HOPS or CSC binding (Nordmann *et al.*, 2010). Our data thus imply that CSC is able to recognize Ypt7 in the context of membranes.

Structure of SNX-BAR and CSC complexes

Structures of human CSC and SNX-BAR have been solved, including the Vps29-Vps35 interface and isolated Vps26 (Collins *et al.*, 2005, 2008; Shi *et al.*, 2006; Hierro *et al.*, 2007), which were used to model the full-length complex (Hierro *et al.*, 2007). For the SNX complexes, structures of the BAR domains of SNX9 and SNX1, the human orthologue of Vps5, are available (Pylypenko *et al.*, 2007; van Weering *et al.*, 2012). To obtain insights into the architecture of the full-length CSC and SNX complexes, we applied purified complexes to gel

filtration columns (Figure 1, C and D). Complexes were analyzed by negative stain microscopy and class averaged, and the overall architecture was determined (Figure 2). For the CSC, we obtained an elongated particle of 15 nm with multiple small extensions (Figure 2, A–C). Taking the human CSC model as a template, we were able to place the crystal structures of Vps29-Vps35 and Vps26 into the density of our structure, unraveling a striking similarity of the human and yeast CSC complexes (Figure 2D). Indeed, the recently solved structure of a fragment of human Vps35 in complex with Vps26 that was published while this work was under review nicely agrees with our findings on the yeast complexes (Lucas *et al.*, 2016). For the SNX-BAR dimer, we observed a large particle of 7 × 15 nm with possible symmetry along the vertical axis (Figure 2, E–G). Our attempt to model the available structure of the human SNX9 into the density failed due to the missing structural information on the large N-terminal segments that precede the PX and SNX-BAR domains. Because the SNX complex functions in the context of membranes, the obtained structure likely reflects the inactive cytosolic form.

Membrane activity of the full-length Vps5-17 SNX-BAR complex

Purified human SNX-BAR proteins can tubulate liposomes, which requires the BAR domain, binding to PI-3-P, and an amphipathic helix (Carlton *et al.*, 2004; van Weering *et al.*, 2012). We used our purified Vps5-17 heterodimer to address its functionality, using liposomes with a simple mixture of phosphatidylcholine, phosphatidylethanolamine, and phosphatidylserine with 1.5 mol% PI-3-P and observed massive tubules of several micrometers by cryo–electron microscopy (Figure 3A). In contrast, the CSC complex did not affect the shape of liposomes (Figure 3A).

To determine membrane activity in a more accessible system, we turned to giant unilamellar vesicles (GUVs). GUVs have been used extensively to determine membrane activity of peripheral membrane proteins (e.g., Itoh *et al.*, 2005; Saarikangas *et al.*, 2009; Meinecke *et al.*, 2013; Numrich *et al.*, 2015). When added to the GUVs, the SNX-BAR heterodimer generated tubules emanating from the GUV surface (Figure 3B), in agreement with our ultrastructural analysis (Figure 3A). On longer incubations, GUVs began to shrink due to the consumption of membranes by tubulation (as seen in Figure 3C). As before, the CSC did not affect GUV morphology (Figure 3B), although we detected some clustering of GUVs at higher concentrations (Figure 4I). To monitor the localization of purified SNX-BAR and CSC complexes directly, we tagged either Vps29 (for CSC) or Vps17 (for SNX-BAR) with green fluorescent protein (GFP), which does not impair their function in vivo (Arlt *et al.*, 2015b). Both complexes were found on GUV membranes (Figure 3, C and D), and SNX-BAR-GFP caused similar tubulation of GUVs as observed for the untagged complex (Figure 3B, quantified in H). When we left out PI-3-P from our GUV preparations, both SNX-BAR binding to the GUV surface and tubulation were lost (Figure 3E). The SNX-BAR heterodimer thus requires PI-3-P binding for membrane recruitment and tubulation activity.
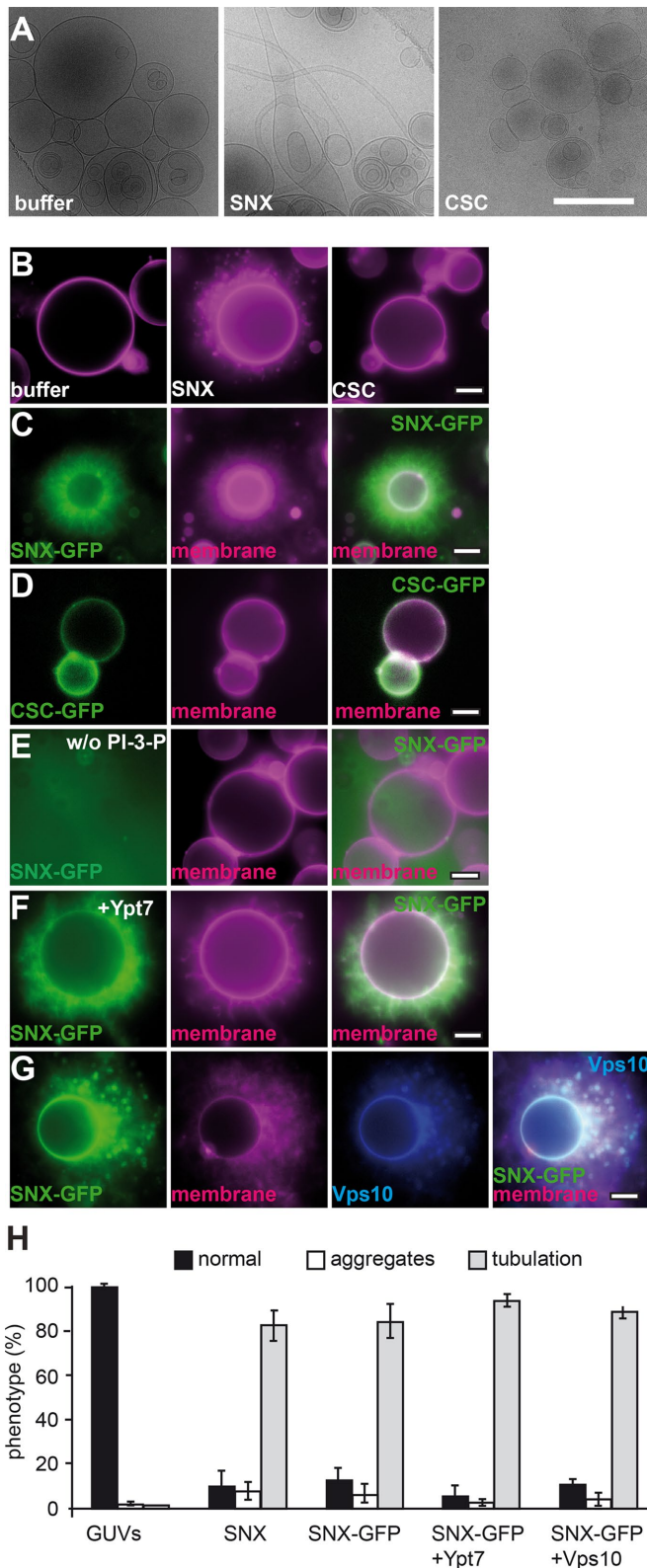
FIGURE 3: Interaction of the SNX-BAR and CSC complexes with membranes. (A) Membrane deformation is induced by purified SNX-BAR complex. Cryo-EM of multilamellar vesicles (MLVs) incubated with buffer, purified SNX-BAR, and CSC. Scale bar, 1 μm. (B) Effect of untagged SNX-BAR and CSC complexes on membrane structure. GUV membranes were incubated in a 30-μl reaction volume in PBS buffer for 15 min at room temperature and then examined by fluorescence microscopy. (C) SNX-BAR complex tubulates GUV

Cargo and Ypt7-GTP affect retromer recruitment

SNX proteins such as SNX3 are important for cargo binding of the retromer (Strochlic *et al.*, 2007; Harterink *et al.*, 2011; Harrison *et al.*, 2014). Structural studies suggested that the CSC subunit Vps26 is the major binding site for cargo (Shi *et al.*, 2006; Collins *et al.*, 2008), which was shown directly for human Vps26 (Fjorback *et al.*, 2012), and others implied direct binding of cargo such as Vps10 to the major CSC subunit Vps35 (Nothwehr *et al.*, 2000). Furthermore, the CSC binds directly to active Rab7/Ypt7 (Rojas *et al.*, 2008; Seaman *et al.*, 2009; Balderhaar *et al.*, 2010; Priya *et al.*, 2015), primarily via its subunit Vps35 (Liu *et al.*, 2012). To unravel the possible assembly of the entire SNX-BAR retromer complex, we charged GUV membranes with cargo and/or Ypt7-GTP. For this, the cytosolic domain of Vps10 (residues 1415–1579) and GTP-loaded Ypt7, both with a C-terminal hexahistidine (His_6) tag, were added to GUVs that carried 1,2-dioleoyl-*sn*-glycero-3-((N-(5-amino-1-carboxypentyl) iminodiacetic acid) succinyl) (DOGS-NTA) lipids to allow binding of the His-tagged protein to the surface. Initially, we monitored whether either protein affects the ability of the SNX-BAR-GFP complex to tubulate membranes, although did not observe any difference (Figure 3, F–H).

Our initial experiments suggested that CSC might not require additional proteins for membrane binding (Figure 3D). However, high concentrations of CSC might have masked crucial membrane requirements for recruitment. Indeed, when we reduced the CSC concentration twofold, CSC-GFP binding to membranes was abolished (Figure 4A). When we added the SNX-BAR complex to this reaction, CSC was efficiently bound to the GUV membrane and began to accumulate in SNX-BAR–induced tubules (Figure 4B). This reaction depended on PI-3-P on the GUV membrane (Figure 4C), in agreement with the PI-3-P–dependent recruitment of the SNX-BAR complex (Figure 3E). We then included Ypt7 and the cargo Vps10 in the reaction. Ypt7 (Figure 4D) or Vps10 (Figure 4G) was sufficient to recruit the CSC complex to membranes also in the absence of PI-3-P (Figure 4F). Of interest, the presence of its ligands seems to suppress CSC-mediated aggregation of GUVs (Figure 4I). As before, addition of the SNX-BAR complex caused the previously observed tubulation of membranes that contained CSC-GFP (Figure 4, E and H; quantified in K). Our data are thus consistent with the idea that CSC and SNX-BAR can bind membranes independently of each other but are found in the same resulting tubular structure. Either Ypt7-GTP or the cargo can strongly enhance CSC binding to membranes, whereas SNX-BAR–dependent tubulation requires PI-3-P. Of importance, CSC is then part of the forming tubule.

SNX-BAR retromer assembly displaces Ypt7 from the retromer

On endosomes, cargo is likely a limiting factor for CSC recruitment. Ypt7/Rab7 binding might therefore be necessary to provide sufficient binding sites to concentrate the CSC on endosomal

membranes. SNX-BAR complex with GFP-tagged Vps17 was incubated with GUV membranes and examined as in B. (D) CSC can bind GUVs. CSC with GFP-tagged Vps29 was added to GUVs and analyzed as before. (E) PI-3-P is required for SNX-BAR membrane association. GUVs lacking PI-3-P were incubated with the same concentration of SNX-BAR complex as in C. (F, G) Effect of surface-bound Ypt7-GTP or Vps10 on SNX tubulation efficiency. GUVs carrying DGS-NTA were incubated with His-tagged Ypt7-GTP or Cy5-labeled Vps10 for 10 min at room temperature before SNX-BAR-GFP was added. Samples were examined by fluorescence microcopy. (H) Quantification of the tubulation efficiency of CSC and SNX-BAR complexes. Data are represented as mean ± SD.
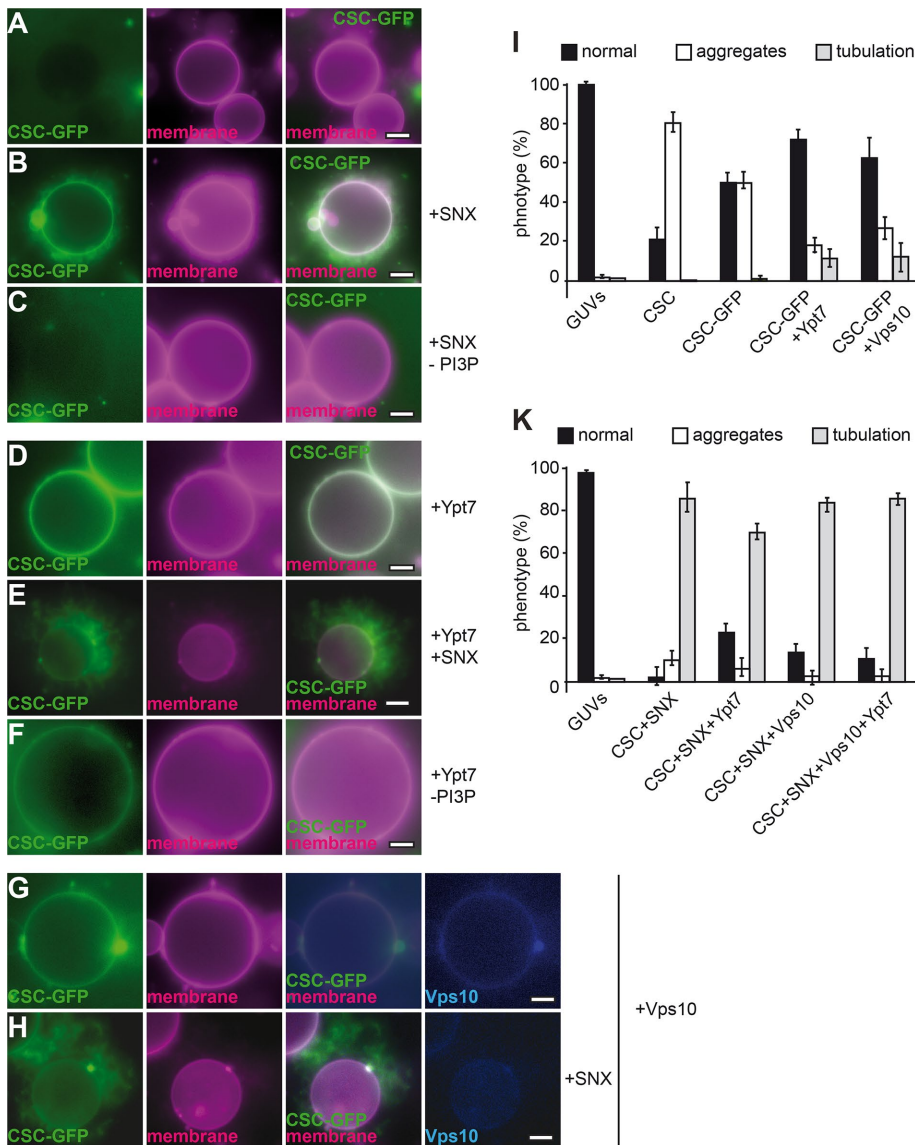
FIGURE 4: Multiple interactions determine CSC membrane binding. (A–C) SNX-BAR interaction can recruit CSC to membranes. Limiting amounts of CSC (corresponding to half the amount in Figure 3D) were incubated with GUV membranes in the absence (A) or presence (B) of untagged SNX complex. In C, GUVs incubated with CSC-GFP and SNX-BAR did not carry PI-3-P. (D–F) Ypt7 binding is sufficient for CSC recruitment. His-tagged Ypt7 was added to GUVs carrying DOGS-NTA before CSC or SNX-BAR complexes were included in the incubation. (D) Binding of CSC-GFP alone. (E) Binding in the presence of untagged SNX-BAR complex. (F) As in E, but without PI-3-P in the GUV preparation. (G, H) Effect of cargo on CSC recruitment. His-tagged Vps10 was labeled with Cy5 as described in *Materials and Methods* and added to GUVs. CSC-GFP was added either alone (G) or with SNX-BAR complex (H) before being analyzed by fluorescence microscopy. (I, K) Quantification of GUV morphology shown in A–H. Data are represented as mean ± SD.

Western blotting. As before, SNX-BAR (Vps17-GFP) did not bind to Ypt7, whereas CSC (Vps29-GFP) selectively bound to Ypt7-GTP (Figure 5A). Strikingly, binding of CSC to Ypt7-GTP was lost as soon as equimolar SNX-BAR was present in the pull-down reaction (Figure 5, A and B), suggesting that assembly of the retromer complex displaces Ypt7. We then used just the N-terminal fragment of Vps5, which has been suggested as a possible interaction site to the CSC (Collins *et al.*, 2005), and also observed loss of CSC binding to Ypt7 (Supplemental Figure S1C). These observations suggest that the interface between SNX-BAR and CSC overlaps with the Ypt7 binding site.

To monitor the displacement of Ypt7 from CSC on membranes, we used a modified GUV-binding assay. As shown before, CSC can be recruited to GUVs by either Ypt7 or Vps10 (Figure 4, D and G). We therefore used Vps10-loaded GUVs to bind CSC to the membrane and then added Ypt7 as a fluorescently labeled but otherwise untagged protein. If SNX-BAR indeed competes with Ypt7 for CSC binding, Ypt7 should be displaced from GUVs if we add the SNX-BAR complex to the reaction. We initially tested Ypt7 binding to the GUV surface and observed CSC- (Figure 5, C and D) and GTP-dependent (Figure 5F) recruitment. Of importance, addition of the SNX-BAR complex to this reaction resulted in a quantitative loss of Ypt7 from the GUV surface (Figure 5, D vs. E), in agreement with Ypt7 displacement from the CSC on assembly of the entire SNX-BAR retromer complex on membranes.

DISCUSSION

Our data provide a molecular explanation for how Ypt7 can participate in two competing interactions on the endosomal surface (Figure 5H). The GEF Mon1-Ccz1 promotes Ypt7 activation on endosomes. 1) CSC then binds Ypt7-GTP and cargo such as the Vps10 receptor, which enhances its ability to localize to endosomes. 2) Endosomes also carry the SNX-BAR complex that interacts with PI-3-P. Assembly of the retromer pentamer from the SNX-BAR and CSC subcomplexes 3) moves cargo into tubular structures and 4) displaces Ypt7 from the CSC. Ypt7-GTP then becomes available for the vacuole-localized HOPS tethering complex, which promotes SNARE-dependent fusion of the mature endosomes with vacuoles.

Our findings have several important implications. Displacement of Ypt7 from endosomal tubules can explain why Ypt7 remains on the donor membrane when retromer tubules are formed (Arlt *et al.*, 2015b). The findings are also consistent with the different vacuole phenotypes of the *vps5Δ* (SNXΔ) and *vps35Δ* (CSCΔ) strains (Liu *et al.*, 2012). Whereas vacuoles in a strain lacking the CSC subunit

membranes. We previously observed by in vivo analyses that Ypt7 remains on the vacuolar rim when SNX-BAR– and CSC-positive tubules emanate from vacuoles (Arlt *et al.*, 2015b). This exclusion could be due to a selective inactivation on tubules by a retromer-recruited GAP (Seaman *et al.*, 2009) or a consequence of the assembly between CSC and SNX-BAR subcomplex during tubule formation. We addressed the latter possibility using Rab pull down with Ypt7-GTP as a readout. For this, the SNX-BAR complex was titrated in a defined molar ratio relative to CSC to the pull-down reaction, and Ypt7-associated CSC was subsequently evaluated by

FIGURE 5: Binding of SNX-BAR to CSC releases Ypt7. (A) Rab interaction of CSC with Ypt7 in the presence of SNX-BAR. Purified CSC and SNX-BAR complexes were incubated with GST-Ypt7 charged with GDP or GTP. For the competition assay, CSC was preincubated with Ypt7 for 15 min before the addition of the indicated relative molar amount of SNX-BAR complex. Incubations on further analysis were as in Figure 1E. (B) Quantification of Rab-CSC interaction; n = 3. (C–G) Interaction of Ypt7 with CSC is reduced upon SNX-BAR addition. GUVs carrying His-tagged Vps10 were incubated with ATTO-labeled Ypt7-GTP or -GDP without His tag (C). In D, GFP-tagged CSC (Vps29-GFP) was added. In E and G, untagged SNX-BAR complex was added to the reaction in a fourfold excess over CSC. In F and G, Ypt7-GDP was used instead of Ypt7-GTP. All images were processed equally. (H) Model of SNX-BAR and CSC interaction with PI-3-P, cargo, and Ypt7. Assembly of the retromer complex displaces Ypt7, thus separating a retromer-positive tubule and a Ypt7-positive membrane. For further details, see the text.

Vps35 are round, they are fragmented in a *vps5Δ* strain, suggesting that the free CSC complex might compete with HOPS for Ypt7, as also observed in our fusion assay (Figure 1, F and G). In agreement

with this, only a small fraction of Ypt7 was found on maturing endosomes (Arlt *et al.*, 2015a), which could initially bind to the CSC before it becomes available for HOPS.

Our data agree with the findings in mammalian cells that CSC and SNX-BAR complexes exist as two separate complexes (Haft *et al.*, 2000; Pylypenko *et al.*, 2007; van Weering *et al.*, 2012). In yeast as well, the SNX-BAR complex seems to localize earlier than the CSC to maturing endosomes (Arlt *et al.*, 2015a), and both can be found on endosomal domains (Chi *et al.*, 2014). We showed here that CSC binds to membranes containing either cargo, Ypt7-GTP or the SNX-BAR complex, in agreement with three binding sites along the Vps29-35-26 trimer (Collins *et al.*, 2005; Liu *et al.*, 2012; Seaman, 2012). The SNX-BAR complex requires PI-3-P for its endosomal recruitment and can efficiently tubulate membranes. Our in vitro assays suggest that assembly of the functional retromer complex during tubule formation occurs from two distinct subcomplexes also in yeast.

In agreement with this analogy, our electron microscopy analysis reveals a striking similarity of the yeast CSC to the human complex (Figure 2). We could easily model all available structures and the Vps35 model into our structure and also show additional segments that agree nicely with the recently solved structure of the CSC (Vps35 and Vps26; Lucas *et al.*, 2016). We can also solve the overall structure of the SNX-BAR complex, which likely reflects the inactive cytosolic conformation of the complex. Because the most complete SNX9 structure with its PX and BAR domain still lacks the first 200 residues (Pylypenko *et al.*, 2007), we refrained from modeling the fragment into our density. The overall assembly of the SNX-BAR retromer cannot yet be deduced from our data, as the heteropenta-meric complex was not suitable for electron microscopy (EM) analysis.

Of interest, although several SNX proteins can act alone to tubu-late membranes (van Weering *et al.*, 2012), their activity seems lower than our full-length Vps5-17 complex, which generated long tubules. We do not yet know whether the tubulation of the SNX-BAR complex has been facilitated by the labile GUV surface, although we also detected strong tubulation of liposomes (Figure 3A). This activity must be controlled in vivo, where the formation of tubules should be a consequence of available cargo and retromer assembly, as also suggested by mutant analyses (Seaman and Williams, 2002). Our present data show the qualitative interdepen-dence between cargo, PI-3-P, and Ypt7 on recruiting retromer sub-complexes. We have, for instance, not yet resolved how cargo is concentrated into retromer-decorated tubules. Further analysis of the organization of assembled retromer on endosomal tubules, as also postulated recently (Lucas *et al.*, 2016), and in particular its cross-talk with cargo, will be important for our understanding of ret-romer function.

The availability of Ypt7-GTP for fusion is likely only one critical parameter that determines maturation of the endosome. It is un-clear how the activity of the ESCRT complexes on ubiquitinated cargo determines fusion competence of endosomes. It appears as if all endosomes are cleared of ESCRT cargoes before fusing with vacuoles. Similarly, the Rab5-like Vps21 is a substrate of the BLOC-1–associated Msb3 protein, and no Vps21 is found on vacuoles in wild-type cells (Lachmann *et al.*, 2012; John Peter *et al.*, 2013; Rana *et al.*, 2015). We consider it likely that retromer, ESCRT, and COR-VET act in parallel on endosomes to promote cargo sorting and fu-sion (Burd and Cullen, 2014; Arlt *et al.*, 2015a). Only if all cargo is taken care of should fusion of late endosomes with the vacuole/lyso-some be initiated. The availability of functional retromer will allow us to resolve this question in future studies.

Genotype		Source
CUY105	*MATa his3Δ200 leu2Δ0 met15Δ0 trp1Δ63 ura3Δ0*	EUROSCARF
CUY100	*MATalpha his3Δ200 leu2Δ0 lys2Δ0 met15Δ0 trp1Δ63 ura3Δ0*	EUROSCARF
CUY9228	CUY105, *VPS5pr::natNT1-GAL1pr VPS17pr::kanMX-GAL1pr VPS5::TAP-URA3 vps35::HIS3*	This study
CUY9495	CUY100, *VPS26pr::HIS3-GAL1pr VPS29pr::natNT2-GAL1pr VPS35pr::hphNT1 VPS35::TAP-kanMX vps5::TRP1 vps17::LEU2*	This study
CUY9711	CUY105, *VPS5pr::natNT1-GAL1pr VPS17pr::kanMX-GAL1pr VPS5::TAP-URA3 vps35::HIS3 VPS17::GFP-hphNT1*	This study
CUY9932	CUY100, *VPS26pr::HIS3-GAL1pr VPS29pr::natNT2-GAL1pr VPS35pr::hphNT1 VPS29::kan VPS26::TAP-URA3 vps5Δ::TRP1*	This study

EUROSCARF, Institute for Molecular Biosciences, Johann Wolfgang Goethe-University Frankfurt, Frankfurt, Germany.

TABLE 1: Strains used in this work.

MATERIALS AND METHODS

Strains and reagents
All reagents were purchased from Sigma-Aldrich, unless noted otherwise. All *Saccharomyces cerevisiae* strains were generated from the respective parent BY strain by integration of PCR-amplified cassettes by homologous recombination as described previously (Longtine *et al.*, 1998; Puig *et al.*, 2001; Janke *et al.*, 2004). Strains are listed in Table 1.

Plasmid generation
The C-terminal fragment (corresponding to amino acid residues 1416–1579) of *VPS10* was amplified from genomic DNA of strain BY4727 and cloned into *Bam*HI, *Sal*I–digested pET32c expression vector to generate plasmid pET32c(-Trx)-VPS10 (1415–1579). The N-terminal fragment of Vps5 (residues 1–280) was amplified by PCR from genomic DNA and cloned into a pET24b expression vector using restriction sites *Nde*I and *Xho*I.

Vacuole fusion assay
Vacuole purification and fusion were performed as previously described (LaGrassa and Ungermann, 2005). In brief, vacuoles were purified from BJ3505 and DKY6281 strains and subjected to vacuole fusion in the presence of ATP. The indicated amounts of CSC and HOPS were added to the fusion reaction, and fusion was determined after 90 min of incubation at 26°C.

Protein purification and labeling
Vps10 and Ypt7 were purified from *Escherichia coli* BL21 (DE3) Rosetta cells expressing plasmids pET32c(-Trx) and pET24b. Cells were lysed in lysis buffer (50 mM 4-(2-hydroxyethyl)-1-piperazineethanesulfonic acid [HEPES]/KOH, 300 mM NaCl, 1 mM MgCl$_2$) supplemented with 0.05× protease inhibitor cocktail (PIC; 1× PIC corresponds to 0.1 μg/ml leupeptin, 0.5 mM *o*-phenanthroline, 0.5 μg/ml pepstatin A, 0.1 mM Pefabloc) and 1 mM phenylmethylsulfonyl fluoride. Lysate was cleared by centrifugation at 20,000 × *g* and subjected to nickel–nitriloacetic acid beads prewashed with lysis buffer containing 20 mM imidazole. Proteins were eluted with buffer containing 300 mM imidazole. Buffer was exchanged to 50 mM HEPES/KOH, pH 7.4, 300 mM NaCl, 1 mM MgCl$_2$, and 10% glycerol using a NAP-10 column (GE Healthcare). For fluorescence labeling of Ypt7 and Vps10, proteins were incubated for 2 h with DY-647 maleimide derivative (Dyomics) or a Cyc-5 amine derivative, respectively, followed by purification on NAP-5 columns.

SNX-BAR and CSC complexes were purified from yeast using tandem affinity purification (TAP) as described (Puig *et al.*, 2001;

Ostrowicz *et al.*, 2010). In brief, strains were grown in rich yeast extract/peptone medium supplemented with 2% galactose for 60 h at 30°C. Cells were lysed in buffer (50 mM Tris/HCl, pH 8.0, 300 mM NaCl, 1.5 mM MgCl$_2$) supplemented with 1 mM dithiothreitol (DTT) and protease inhibitor FY (Roche, Munich), and lysate was cleared by centrifugation at 4°C for 5 min at 3500 × *g* and then for 1 h at 50,000 × *g*. Cleared lysate was incubated with immunoglobulin G (IgG)–Sepharose beads (GE Healthcare) at 4°C for 1 h, followed by elution using tobacco etch virus (TEV) protease at 16°C for 90 min, and then used in subsequent assays, including EM. Where indicated, purified complexes were subjected to size-exclusion chromatography on a Superose 6 10/300 column (GE Healthcare).

Liposome and GUV preparations
All lipids were purchased from Avanti Polar Lipids. Liposomes were generated by mixing 1,2-dioleoyl-*sn*-glycerol-3-phosphocholine (40.2 mol%), 1,2-dioleoyl-*sn*-glycerol-3-phosphoethanolamine (7.5 mol%), 1,2-dioleoyl-*sn*-glycerol-3-phospho-L-serine (5.35 mol%), the lipid dye ATTO 550 (0.5 mol%), and, where indicated, DOGS-NTA (nickel salt; 2.5 mol%) and PI-3-P (diC16; 1.5 mol%), in chloroform:methanol (2:1). Organic solvent was evaporated, and lipids were resuspended in buffer (50 mM HEPES/KOH, pH 7.2, 120 mM KOAc), followed by nine freeze/thaw cycles in liquid nitrogen.

GUVs were prepared using an electroformation protocol as described in Romanov *et al.* (2012). Briefly, the desired lipid mix (concentration 2 mM in 500 μl) was dissolved in a chloroform:methanol (2:1) solution, and 3 μl was spotted onto prewashed indium tin oxide–coated slides. Organic solvent was removed in vacuum, and slides were assembled to create a chamber for 500 μl of 300 mM sucrose, followed by electroformation using Vesicle Prep Pro (Nanion, Munich, Germany) in a 3-h cycle. GUVs were centrifuged onto a sucrose cushion at 120 × *g* for 20 min at 4°C using sedimentation buffer (1 mM HEPES/KOH, pH 7.4, 267 mM glucose, 1 mM DTT). The cushion consisted of sedimentation and swelling buffer (1 mM HEPES/KOH, pH 7.4, 240 mM sucrose, 1 mM DTT) mixed 1:1. GUVs were taken up into a final volume of 5 μl, resulting in a final concentration of 0.2 mM.

GUV assays and fluorescence microscopy
To determine protein binding and membrane deformation by retromer complexes, purified CSC or SNX-BAR complexes were used at a final concentration of 100–150 nM in the reaction. The complexes were first added to 5 μl of the concentrated GUVs (0.2 mM) in a final volume of 30 μl in phosphate-buffered saline (PBS) and then

incubated for 15 min before examination by microscopy. Preloading of GUVs with GTP- or GDP-loaded Ypt7 or Vps10 was carried out by incubating GUVs for 20 min at room temperature with 0.5 μM each protein.

GUVs were imaged on an Olympus IX-71 inverted microscope using 60×/numerical aperture (NA) 1.40 and 100×/NA 1.49 objectives, InsightSSI illumination, a scientific complementary metal-oxide semiconductor camera (PCO), and SoftWoRx software (Applied Precision). Usually, z-stacks of 0.2 μm in 15 optical slices to cover a total of 3 μm were acquired, followed by deconvolution using SoftWoRx software and image processing in ImageJ (National Institutes of Health, Bethesda, MD). GUV morphology was quantified by counting at least 50 GUVs per sample in three independent experiments.

Rab pull-down assay

The glutathione-Rab pull-down experiment was carried out as described (Markgraf *et al.*, 2009). Recombinant GST-tagged Rab proteins were loaded with 1 mM GDP/GTP in 20 mM HEPES/NaOH, pH 7.4, and 20 mM EDTA and subsequently incubated with GST beads (pretreated with the same buffer containing 5% bovine serum albumin) for 1 h at 4°C. Beads were washed, and retromer complexes (20–40 μg) were added for 1.5 h in 20 mM HEPES/NaOH, pH 7.4, 300 mM NaCl, and 1 mM MgCl$_2$, followed by washing in buffer and elution by addition of 20 mM EDTA, 0.1% Triton X-100. Proteins in eluates were precipitated by trichloroacetic acid and analyzed by SDS–PAGE and Western blotting.

Electron microscopy and image processing

Purified protein samples were negatively stained with 0.035 mg/ml uranyl formate according to a previously described protocol (Ohi *et al.*, 2004). The micrographs were collected with a charge-coupled device camera (Tvips, 4k × 4k) integrated into a Jeol JEM-1400 with LaB6 cathode at 120 kV. After manual selection of the single particles, reference-free and reference-based alignment, as well as K-means and ISAC classification, were performed with EMAN2 and SPARX. For three-dimensional (3D) reconstruction of the CSC, random conical tilt data were collected at −50 and 0°. We selected 2707 particle pairs using EMAN2 e2RCTboxer tool. All untilted particles were aligned and classified with EMAN2 and SPARX. A 3D model was calculated from different classes using the corresponding tilted particles. The resulting model was submitted to 3D multireference projection matching against the data set of 9875 single particles using SPARX. The 3D model of SNX was calculated with the VIPER algorithm. We aligned 2245 particles and classified K-means into 50 classes. These provided the template for ab initio 3D structure determination with sxviper (SPARX). The initial model was refined subsequently with the single particles.

For liposome cryo–EM, retromer complexes and liposomes were incubated for 1 h at room temperature before a 4-μl sample was applied on a Quantifoil 2/1 holey carbon grid, blotted from both sides with Whatman1 for 3.5 s, and plunged into liquid ethane using Cryoplunge3 with GentleBlot technology. The vitrified samples were imaged with a Jeol JEM-3200FSC electron microscope operating with a field emission gun at 200 kV. An in-column omega energy filter was used to improve image contrast by zero-loss filtering with a slit width of 15 eV. Micrographs were recorded for 3 s as 15 frame stacks with a K2 camera (Gatan) under minimal-dose conditions (20 e⁻/Å^2; Li *et al.*, 2013).

REFERENCES

Arlt H, Auffarth K, Kurre R, Lisse D, Piehler J, Ungermann C (2015a). Spatiotemporal dynamics of membrane remodeling and fusion proteins during endocytic transport. Mol Biol Cell 26, 1357–1370.

Arlt H, Reggiori F, Ungermann C (2015b). Retromer and the dynamin Vps1 cooperate in the retrieval of transmembrane proteins from vacuoles. J Cell Sci 128, 645–655.

Balderhaar HJK, Arlt H, Ostrowicz CW, Bröcker C, Sündermann F, Brandt R, Babst M, Ungermann C (2010). The Rab GTPase Ypt7 is linked to retromer-mediated receptor recycling and fusion at the yeast late endosome. J Cell Sci 123, 4085–4094.

Balderhaar HJK, Ungermann C (2013). CORVET and HOPS tethering complexes—coordinators of endosome and lysosome fusion. J Cell Sci 126, 1307–1316.

Barr FA (2013). Review series: Rab GTPases and membrane identity: causal or inconsequential? J Cell Biol 202, 191–199.

Burd C, Cullen PJ (2014). Retromer: a master conductor of endosome sorting. Cold Spring Harb Perspect Biol 6, a016774.

Burda P, Padilla SM, Sarkar S, Emr SD (2002). Retromer function in endosome-to-Golgi retrograde transport is regulated by the yeast Vps34 PtdIns 3-kinase. J Cell Sci 115, 3889–3900.

Carlton J, Bujny M, Peter BJ, Oorschot VMJ, Rutherford A, Mellor H, Klumperman J, McMahon HT, Cullen PJ (2004). Sorting nexin-1 mediates tubular endosome-to-TGN transport through coincidence sensing of high-curvature membranes and 3-phosphoinositides. Curr Biol 14, 1791–1800.

Chi RJ, Liu J, West M, Wang J, Odorizzi G, Burd CG (2014). Fission of SNX-BAR-coated endosomal retrograde transport carriers is promoted by the dynamin-related protein Vps1. J Cell Biol 202, 527.

Collins BM, Norwood SJ, Kerr MC, Mahony D, Seaman MNJ, Teasdale RD, Owen DJ (2008). Structure of Vps26B and mapping of its interaction with the retromer protein complex. Traffic 9, 366–379.

Collins BM, Skinner CF, Watson PJ, Seaman MNJ, Owen DJ (2005). Vps29 has a phosphoesterase fold that acts as a protein interaction scaffold for retromer assembly. Nat Struct Mol Biol 12, 594–602.

Cullen PJ, Korswagen HC (2012). Sorting nexins provide diversity for retromer-dependent trafficking events. Nat Cell Biol 14, 29–37.

Fjorback AW, Seaman M, Gustafsen C, Mehmedbasic A, Gokool S, Wu C, Militz D, Schmidt V, Madsen P, Nyengaard JR, *et al.* (2012). Retromer binds the FANSHY sorting motif in SorLA to regulate amyloid precursor protein sorting and processing. J Neurosci 32, 1467–1480.

Griffith J, Reggiori F (2009). Ultrastructural analysis of nanogold-labeled endocytic compartments of yeast Saccharomyces cerevisiae using a cryosectioning procedure. J Histochem Cytochem 57, 801–809.

Haas A, Conradt B, Wickner W (1994). G-protein ligands inhibit in vitro reactions of vacuole inheritance. J Cell Biol 126, 87–97.

Haft CR, la Luz Sierra de M, Bafford R, Lesniak MA, Barr VA, Taylor SI (2000). Human orthologs of yeast vacuolar protein sorting proteins Vps26, 29, and 35: assembly into multimeric complexes. Mol Biol Cell 11, 4105–4116.

Harrison MS, Hung CS, Liu TT, Christiano R, Walther TC, Burd CG (2014). A mechanism for retromer endosomal coat complex assembly with cargo. Proc Natl Acad Sci USA 111, 267–272.

Harterink M, Port F, Lorenowicz MJ, McGough IJ, Silhankova M, Betist MC, van Weering JRT, van Heesbeen RGHP, Middelkoop TC, Basler K, *et al.* (2011). A SNX3-dependent retromer pathway mediates retrograde transport of the Wnt sorting receptor Wntless and is required for Wnt secretion. Nat Cell Biol 13, 914–923.

Henne WM, Buchkovich NJ, Emr SD (2011). The ESCRT pathway. Dev Cell 21, 77–91.

Hierro A, Rojas AL, Rojas R, Murthy N, Effantin G, Kajava AV, Steven AC, Bonifacino JS, Hurley JH (2007). Functional architecture of the retromer cargo-recognition complex. Nature 449, 1063–1067.

Huotari J, Helenius A (2011). Endosome maturation. EMBO J 30, 3481–3500.

Itoh T, Erdmann KS, Roux A, Habermann B, Werner H, de Camilli P (2005). Dynamin and the actin cytoskeleton cooperatively regulate plasma membrane invagination by BAR and F-BAR proteins. Dev Cell 9, 791–804.

Jahn R, Scheller R (2006). SNAREs—engines for membrane fusion. Nat Rev Mol Cell Biol 7, 631–643.

Janke C, Magiera MM, Rathfelder N, Taxis C, Reber S, Maekawa H, Moreno-Borchart A, Doenges G, Schwob E, Schiebel E, Knop M (2004). A versatile toolbox for PCR-based tagging of yeast genes: new fluorescent proteins, more markers and promoter substitution cassettes. Yeast 21, 947–962.

John Peter AT, Lachmann J, Rana M, Bunge M, Cabrera M, Ungermann C (2013). The BLOC-1 complex promotes endosomal maturation by recruiting the Rab5 GTPase-activating protein Msb3. J Cell Biol 201, 97–111.

Kinchen JM, Ravichandran KS (2010). Identification of two evolutionarily conserved genes regulating processing of engulfed apoptotic cells. Nature 464, 778–782.

Kümmel D, Ungermann C (2014). Principles of membrane tethering and fusion in endosome and lysosome biogenesis. Curr Opin Cell Biol 29C, 61–66.

Lachmann J, Barr FA, Ungermann C (2012). The Msb3/Gyp3 GAP controls the activity of the Rab GTPases Vps21 and Ypt7 at endosomes and vacuoles. Mol Biol Cell 23, 2516–2526.

LaGrassa TJ, Ungermann C (2005). The vacuolar kinase Yck3 maintains organelle fragmentation by regulating the HOPS tethering complex. J Cell Biol 168, 401–414.

Li X, Mooney P, Zheng S, Booth CR, Braunfeld MB, Gubbens S, Agard DA, Cheng Y (2013). Electron counting and beam-induced motion correction enable near-atomic-resolution single-particle cryo-EM. Nat Methods 10, 584–590.

Li Y, Li B, Liu L, Chen H, Zhang H, Zheng X, Zhang Z (2015). FgMon1, a guanine nucleotide exchange factor of FgRab7, is important for vacuole fusion, autophagy and plant infection in Fusarium graminearum. Sci Rep, doi: 10.1038/srep18101.

Liu TT, Gomez TS, Sackey BK, Billadeau DD, Burd CG (2012). Rab GTPase regulation of retromer-mediated cargo export during endosome maturation. Mol Biol Cell 23, 2505–2515.

Longtine M, McKenzie A, Demarini D, Shah N, Wach A, Brachat A, Philippsen P, Pringle J (1998). Additional modules for versatile and economical PCR-based gene deletion and modification in Saccharomyces cerevisiae. Yeast 14, 953–961.

Lucas M, Gershlick DC, Vidaurrazaga A, Rojas AL, Bonifacino JS, Hierro A (2016). Structural mechanism for cargo recognition by the retromer complex. Cell 167, 1623–1635.e14.

Markgraf DF, Ahnert F, Arlt H, Mari M, Peplowska K, Epp N, Griffith J, Reggiori F, Ungermann C (2009). The CORVET subunit Vps8 cooperates with the Rab5 homolog Vps21 to induce clustering of late endosomal compartments. Mol Biol Cell 20, 5276–5289.

Meinecke M, Boucrot E, Çamdere G, Hon WC, Mittal R, McMahon HT (2013). Cooperative recruitment of dynamin and BIN/amphiphysin/Rvs (BAR) domain-containing proteins leads to GTP-dependent membrane scission. J Biol Chem 288, 6651–6661.

Nordmann M, Cabrera M, Perz A, Bröcker C, Ostrowicz CW, Engelbrecht-Vandré S, Ungermann C (2010). The Mon1-Ccz1 complex is the GEF of the late endosomal Rab7 homolog Ypt7. Curr Biol 20, 1654–1659.

Nothwehr S, Ha S, Bruinsma P (2000). Sorting of yeast membrane proteins into an endosome-to-golgi pathway involves direct interaction of their cytosolic domains with Vps35p. J Cell Biol 151, 297–310.

Numrich J, Péli-Gulli MP, Arlt H, Sardu A, Griffith J, Levine T, Engelbrecht-Vandré S, Reggiori F, de Virgilio C, Ungermann C (2015). The I-BAR protein Ivy1 is an effector of the Rab7 GTPase Ypt7 involved in vacuole membrane homeostasis. J Cell Sci 128, 2278–2292.

Ohi M, Li Y, Cheng Y, Walz T (2004). Negative staining and image classification - powerful tools in modern electron microscopy. Biol Proced Online 6, 23–34.

Ostrowicz CW, Bröcker C, Ahnert F, Nordmann M, Lachmann J, Peplowska K, Perz A, Auffarth K, Engelbrecht-Vandré S, Ungermann C (2010). Defined subunit arrangement and rab interactions are required for functionality of the HOPS tethering complex. Traffic 11, 1334–1346.

Poteryaev D, Datta S, Ackema K, Zerial M, Spang A (2010). Identification of the switch in early-to-late endosome transition. Cell 141, 497–508.

Prescianotto-Baschong C, Riezman H (2002). Ordering of compartments in the yeast endocytic pathway. Traffic 3, 37–49.

Priya A, Kalaidzidis IV, Kalaidzidis Y, Lambright D, Datta S (2015). Molecular insights into Rab7-mediated endosomal recruitment of core retromer: deciphering the role of Vps26 and Vps35. Traffic 16, 68–84.

Puig O, Caspary F, Rigaut G, Rutz B, Bouveret E, Bragado-Nilsson E, Wilm M, Seraphin B (2001). The tandem affinity purification (TAP) method: a general procedure of protein complex purification. Methods 24, 218–229.

Pylypenko O, Lundmark R, Rasmuson E, Carlsson SR, Rak A (2007). The PX-BAR membrane-remodeling unit of sorting nexin 9. EMBO J 26, 4788–4800.

Rana M, Lachmann J, Ungermann C (2015). Identification of a Rab GTPase-activating protein cascade that controls recycling of the Rab5 GTPase Vps21 from the vacuole. Mol Biol Cell 26, 2535–2549.

Rojas R, van Vlijmen T, Mardones GA, Prabhu Y, Rojas AL, Mohammed S, Heck AJ, Raposo G, van der Sluijs P, Bonifacino JS (2008). Regulation of retromer recruitment to endosomes by sequential action of Rab5 and Rab7. J Cell Biol 183, 513–526.

Romanov J, Walczak M, Ibiricu I, Schüchner S, Ogris E, Kraft C, Martens S (2012). Mechanism and functions of membrane binding by the Atg5-Atg12/Atg16 complex during autophagosome formation. EMBO J 31, 4304–4317.

Saarikangas J, Zhao H, Pykäläinen A, LaurinmAki P, Mattila PK, Kinnunen PKJ, Butcher S J, Lappalainen P (2009). Molecular mechanisms of membrane deformation by I-BAR domain proteins. Curr Biol 19, 95–107.

Seaman M, Williams H (2002). Identification of the functional domains of yeast sorting nexins Vps5p and Vps17p. Mol Biol Cell 13, 2826–2840.

Seaman MNJ (2004). Cargo-selective endosomal sorting for retrieval to the Golgi requires retromer. J Cell Biol 165, 111–122.

Seaman MNJ (2012). The retromer complex—endosomal protein recycling and beyond. J Cell Sci 125, 4693–4702.

Seaman MNJ, Gautreau A, Billadeau DD (2013). Retromer-mediated endosomal protein sorting: all WASHed up! Trends Cell Biol 23, 522–528.

Seaman MNJ, Harbour ME, Tattersall D, Read E, Bright N (2009). Membrane recruitment of the cargo-selective retromer subcomplex is catalysed by the small GTPase Rab7 and inhibited by the Rab-GAP TBC1D5. J Cell Sci 122, 2371–2382.

Seaman MNJ, McCaffery JM, Emr SD (1998). A membrane coat complex essential for endosome-to-Golgi retrograde transport in yeast. J Cell Biol 142, 665–681.

Shi H, Rojas R, Bonifacino JS, Hurley JH (2006). The retromer subunit Vps26 has an arrestin fold and binds Vps35 through its C-terminal domain. Nat Struct Mol Biol 13, 540–548.

Singh MK, Krüger F, Beckmann H, Brumm S, Vermeer JEM, Munnik T, Mayer U, Stierhof YD, Grefen C, Schumacher K, Jürgens G (2014). Protein delivery to vacuole requires SAND protein-dependent Rab GTPase conversion for MVB-vacuole fusion. Curr Biol 24, 1383–1389.

Strochlic TI, Setty TG, Sitaram A, Burd CG (2007). Grd19/Snx3p functions as a cargo-specific adapter for retromer-dependent endocytic recycling. J Cell Biol 177, 115–125.

Toshima JY, Toshima J, Kaksonen M, Martin AC, King DS, Drubin DG (2006). Spatial dynamics of receptor-mediated endocytic trafficking in budding yeast revealed by using fluorescent alpha-factor derivatives. Proc Natl Acad Sci USA 103, 5793–5798.

van Weering JRT, Sessions RB, Traer CJ, Kloer DP, Bhatia VK, Stamou D, Carlsson SR, Hurley JH, Cullen PJ (2012). Molecular basis for SNX-BAR-mediated assembly of distinct endosomal sorting tubules. EMBO J 31, 4466–4480.

Wickner W (2010). Membrane fusion: five lipids, four SNAREs, three chaperones, two nucleotides, and a Rab, all dancing in a ring on yeast vacuoles. Annu Rev Cell Dev Biol 26, 115–136.

Yousefian J, Troost T, Grawe F, Sasamura T, Fortini M, Klein T (2013). Dmon1 controls recruitment of Rab7 to maturing endosomes in Drosophila. J Cell Sci 126, 1583–1594.